DOI 10.2478/ama-2023-0002

CHALLENGES IN THE DESIGN OF A NEW CENTRIFUGAL FAN WITH VARIABLE IMPELLER GEOMETRY

Piotr ODYJAS*, Jędrzej WIĘCKOWSKI*, Damian PIETRUSIAK*, Przemyslaw MOCZKO*

*Faculty of Mechanical Engineering, Department of Machine Design and Research, Wroclaw University of Science and Technology, ul. Łukasiewicza 7/9, 50-371 Wrocław, Poland

piotr.odyjas@pwr.edu.pl, jedrzej.wieckowski@pwr.edi.pl, damian.pietrusiak@pwr.edu.pl, przemyslaw.moczko@pwr.edu.pl

received 1 July 2022, revised 27 September 2022, accepted 4 October 2022

Abstract: This article presents a description of design work for newly created centrifugal fans. This was done based on the example of an innovative solution that uses a change in impeller geometry. In the described solution, this is achieved by shortening and lengthening the impeller blades. The development of a technical solution with such properties requires a change of approach in the design process compared with classic solutions. Therefore, the following text describes this process from the concept stage to demonstrator tests. The principle of operation of such a solution is presented and the assumptions made based on analytical calculations are also described. The text also shows a 3D model of the centrifugal fan with variable impeller geometry, made with the help of computer aided design (CAD) tools. In the further part, numerical calculations were made on its basis. The finite element method (FEM) calculation made it possible to verify the structural strength of the project and its modal properties as well as to verify flow parameters, thanks to the use of computational fluid dynamics (CFD) calculations. The next step describes the procedure for testing centrifugal fans with variable rotor geometry, which is different from that of fans without this feature. The next part presents the results of research from the tests carried out.

Key words: centrifugal fan, adjustable fan blade, efficiency, field tests

1. INTRODUCTION

The current trend to use more and more efficient machines and environmentally friendly ones push for the development of numerous technological devices. A similar situation applies to rotary machines, which include, among others, fans. The principle of operation and construction of fans has not undergone significant changes for years. Truly, fans made of light or artificial metals are currently appearing on the market, but the principle of their work is still the same.

The problem of fans operating in changing conditions seems to be still a challenging task for fan users and designers. Basically, the fan is applied to installation according to one, nominal working point in which the fan should have the best possible efficiency. Unfortunately in many cases, the fan is used in installations where changes in the flow parameters take place in time. In such cases, it is expected to ensure that fan can be operated still with relatively high efficiency. Generally, there are two main solutions applied in the case of centrifugal fans that need to be regulated. These are regulated by a change of the rotational velocity with the use of frequency inverter and radial vane inlet control (RVIC) system, where the change of the fan characteristic occurs due to a swirl formed in the fan inlet duct. The first solution generally ensures the best efficiency of the fan with the regulation in a wide range [1–6].

Other solutions that were proposed within years are less efficient or more demanding from the point of view of difficulties in their design or manufacturing. In the first group, there are such solutions as fan regulation with the use of throttling devices (especially in outlet ducts) and fan regulation with the use of a variable geometry system. These are the mainly used two control systems. The first one is the regulation by change of the blade width, which causes a shift of the fan pressure curve in direction of lower (narrower impeller width) or higher (wider impeller width) flow rate values. The second solution is based on the change of the trailing edge angle of the blade. It is realised by rotation of the movable blade end in upward or downward directions. Definitely, as shown by currently gathered knowledge, the first solution is much less efficient than the second one [1–9].

In contrast to both mentioned solutions with regulation method via variable geometry, we proposed a completely new idea of centrifugal fan regulation [10]. This solution is based on the fact that the change in the blade length causes a change in the amount of energy inverted within the impeller. The lengthening or shortening of the blade length also causes a change in the impeller outlet diameter D2 and a change of the velocity triangle on the trailing edge. It leads to a change in the flow parameters and the characteristics of the centrifugal fan. This simple idea is presented in Fig. 1.

In this article, we describe the designing process of this new fan from its conception to manufacturing and testing of the prototype. This work widens knowledge about regulation methods, their drawbacks and possible application.

2. ANALYTICAL CALCULATIONS

In the first step, analytical calculations have been used to design the geometry of the basic fan. This basic geometry was

then used to find the geometry of the fan with the variable geometry. The variability of the basic blade trailing edge diameter D2, as well as blade length *l*, has been assumed as ±10% of deviations from their basic values. On this basis, the design and calculation of the steering mechanism for the adjustment of the blade during movement or standstill were made. In this case, computational methods from the theory of the construction of machines and mechanisms were used. The following subsections present the results of each step of the calculation.

2.1. Evaluation of the basic geometry of the centrifugal fan

In the first stages of the project, it was assumed that the designed centrifugal fan at its basic operating point had a total pressure rise of $\Delta pt = 2500$ Pa and volumetric flow rate $V = 2.78$ m³/s, with the nominal rotational speed $n = 1500$ rpm. On this basis, the preliminary geometry of the new fan has been designed with the use of analytical methods described in the literature [3–6]. As a result, following geometrical data of the impeller have been defined (Fig. 1):

- inlet bore diameter D0 = 384.5 mm;
- blade inlet diameter D1 = D0;
- blade outer diameter D2 = 810 mm;
- diameter of disc and cover of the impeller D22 = 820 mm;
- the width of the blade on the diameter D1: b1 = 172 mm;
- the width of the blade on the diameter D2: b2 = 123 mm;
- blade leading edge angle: ®1 = 24°;
- trailing edge angle: ®2 = 29°;
- number of blades: *z* = 12.

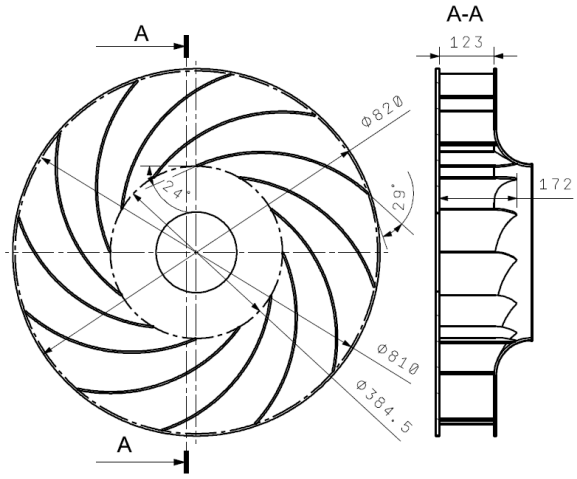

Fig. 1. Main dimensions of the basic impeller

The length of the blade *l* in the basic impeller is equal to 410.33 mm. Assuming that the change of the D2 diameter in the newly designed fan should be in the range of ±10%, it means that the minimal D2min diameter is equal to 729 mm and the maximal D2max diameter is equal to 891 mm. Then, resultant blade lengths in minimal and maximal positions will be $l_{min} = 369.30$ mm and $l_{max} = 451.36$ mm, respectively. The geometry of the impeller with a blade in minimal, basic (middle) and maximal positions is shown in Figs 2–4. Apart from the calculations of the impeller, dimensions of the volute casing have been defined. The geometrical model of this casing is shown in Fig. 5. The fan inlet diameter is 450 mm and the outlet hole from the volute is 355 mm x 450 mm. The width of the volute casing is equal to 355 mm.

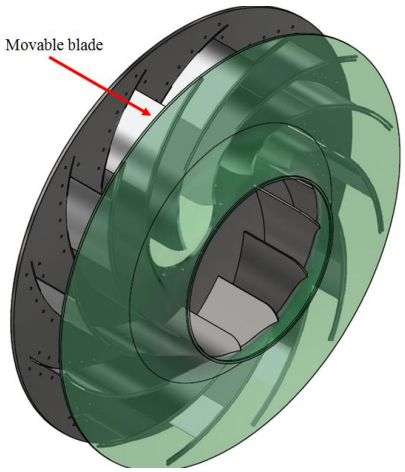

Fig. 2. Geometrical model of the centrifugal fan impeller with the movable blade in the basic (middle) position

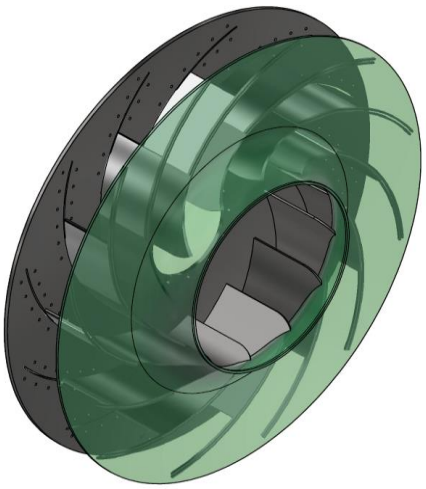

Fig. 3. Geometrical model of the centrifugal fan impeller with the movable blade in minimal position

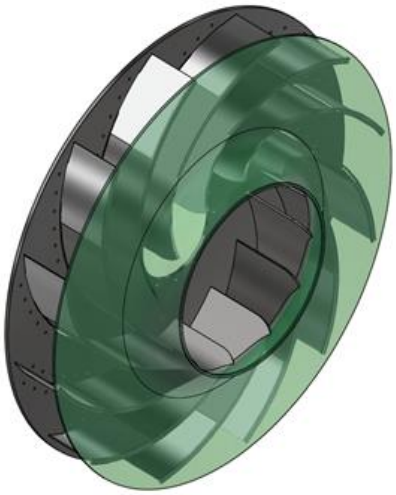

Fig. 4. Geometrical model of the centrifugal fan impeller with the movable blade in maximal position

DOI 10.2478/ama-2023-0002

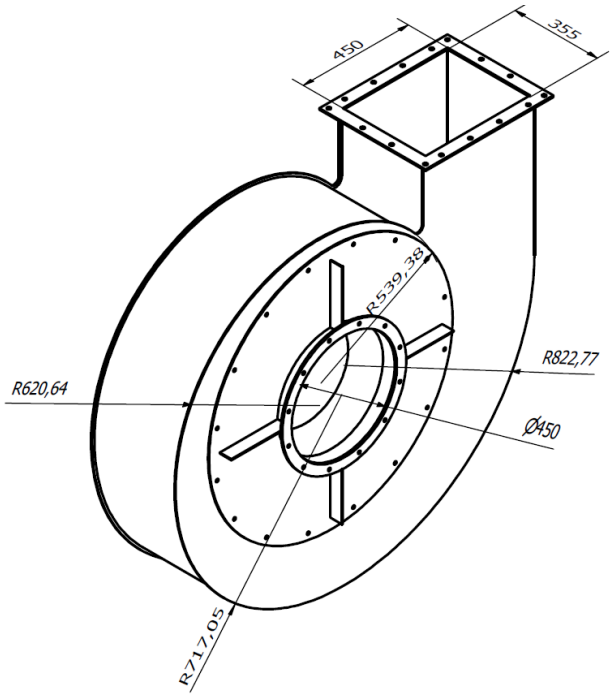

Fig. 5. Geometrical model of the designed centrifugal fan volute casing with main dimensions

2.2. Calculations and description of the steering mechanism

The calculations of the forces acting on the main elements of the steering system were carried out based on the relevant literature [11, 12]. First, the maximum forces acting on the blade supports (pos. 5 and 6, Fig. 6) were calculated, derived from the centrifugal force related to the mass of the movable part of the blade (pos. 2, Fig. 6). The mechanism in the final version is shown in Figs 6 and 7. The translation of the movable blade (pos. 2, Fig. 6) is executed, along rails (pos. 5 and 6, Fig. 6), by the tie rod (pos. 3, Fig. 6). The movement of the strand is possible as a result of the rotary motion of the steering disc (item 4, Fig. 6). The movement of the steering disk is relative to the rotating shaft and hub of the fan. The control disc is rotated (in relation to the shaft) by the link (item 8, Fig. 7), the movement of which is generated by the positive coupling of the link with the adjusting drum (item 9, Fig. 7). The positive connection of the link with the drum is realised through the slots of the helical track, which in fact enables the axial movement of the drum along the shaft to be changed to the angular movement of the link. The axial movement of the drum is ensured by a screw drive independent of the fan drive system. The position of the fan blades can be controlled during operation and at a standstill position of the fan. The designed solution of the moving blade system has special handles for each blade (pos. 7, Fig. 6). This handle is also a slider on 2D rails (pos. 6, Fig. 6).

The performed FEM calculations allowed for precise shaping of the blade made of an aluminum alloy with a thickness of 2 mm. The shape of the blade in the final solution is shown in Fig. 8. Its weight is equal to 213 g. Based on this mass, the forces acting on the tie rod and other elements were calculated, assuming that the friction coefficient between the sliding elements was relatively high and amounted to 0.5. Finally, the axial force that must be applied on the drum to move the blade from the maximum position was calculated and it is 12 kN.

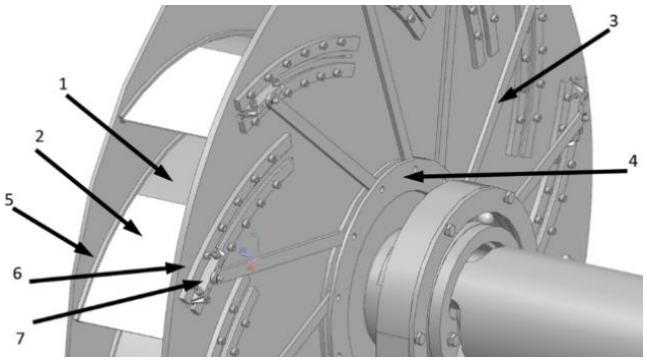

Fig. 6. Impeller geometry with tie rods mechanism—parts mounted to the impeller

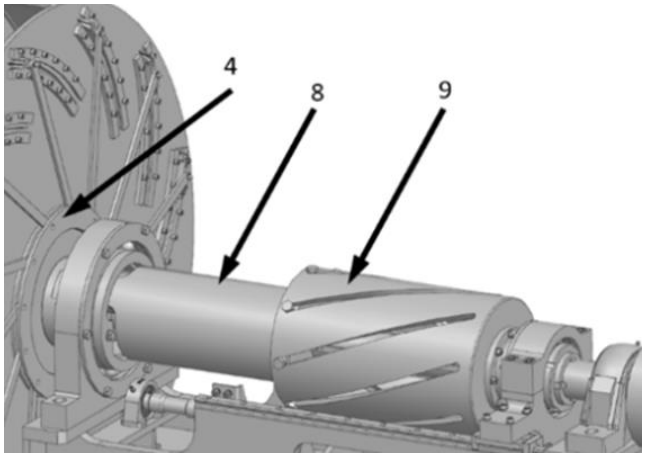

Fig. 7. Impeller geometry with tie rods mechanism—parts mounted on the drive shaft

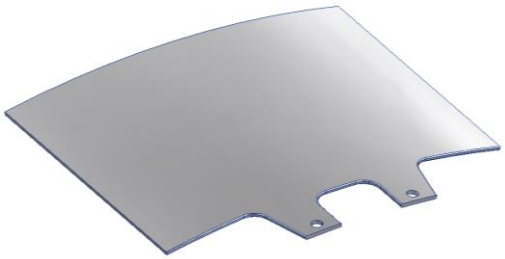

Fig. 8. Final form of the geometrical shape of the movable blade

3. NUMERICAL CALCULATIONS

CAD tools are currently one of the most popular solutions for designing process support. They allow for the integration of work on the shape of the developed solution with strength calculations. In the case of technical devices responsible for the transport of liquids and gases, flow calculations are also important. They are also currently being made with a CAD tool. The following subsections present the effects of individual verification stages of the project.

3.1. Geometrical model

Based on the preliminary choice of the geometry type and dimensions, with further calculations of the mechanism done, the

3D geometrical model of the fan was prepared. The whole model of the designed fan is shown in Fig. 9. In Figs 5–8, the model of the volute casing, impeller with adjusting mechanism and the final shape of the movable blade are shown. This model was used to check if there are any collisions between moving parts in the model to prevent serious problems after manufacturing the fan. The main parts of the fan that are subject to high inertia forces (rotating parts) and resultant forces in the mechanism have been optimised with the use of FE analysis. A simplified model of the impeller was also used for preliminary CFD calculations to calculate fan performance curves. It was needed to estimate the range of operation of the newly designed fan.

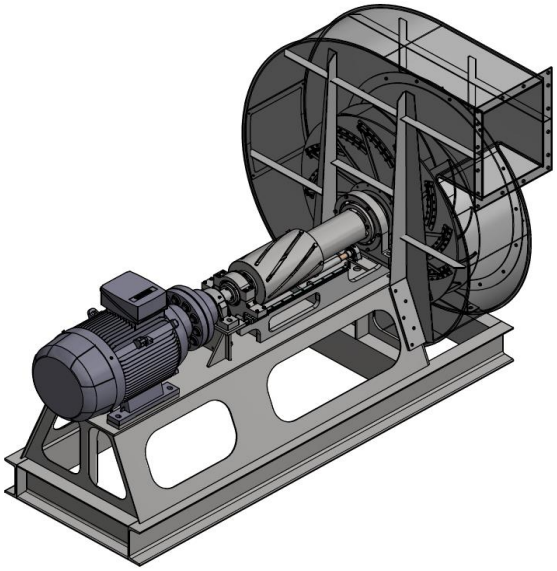

Fig. 9. 3-D geometrical model of the whole fan designed during the project

Ultimately, based on the geometrical mode and results of numerical simulations, technical drawings of the fan have been prepared to enable manufacturing of the fan prototype with a new regulation method.

3.2. FEM simulations

Based on this step, the calculation of the most vulnerable components of the fan with the use of FE analysis has been carried out. The main intention was to check if any of these components are sufficiently resistant to loads acting during fan and mechanism operation. These components were any rotating parts (impeller parts and others from adjusting mechanism) and other components of the fan that were subject to load. Due to the quite complicated mechanism of adjusting the position of the movable blades, the calculations to ascertain the strength were carried out independently for the individual components of the fan. The loads acting on these elements were determined based on analytical calculations, taking into account the kinematics of the system and the maximum operational loads (rotational speed). This approach is used to limit the size of the analysis by limiting the size of numerical models, while correctly refining the finite element mesh. In the case of modal analysis, FEM calculations were carried out for the entire fan rotor assembly to correctly identify the frequency and mode of natural vibrations. On the other hand, the bolted connections used in the fan were carried out analytically.

In case when the strength of fan components was not sufficient, the geometry of that component has been optimised. If modifications of the geometry did not succeed, more rigid materials have been chosen for such components. That was especially visible in the case of the blade, adjusting drum and connector.

In the first step, with the use of the geometrical model, the discrete model of the calculated components has been prepared according to the best practices [13–15]. These were mostly solid models to ensure a more detailed assessment. After that proper boundary conditions have been applied and an enabled numerical simulation was run. Exemplary mesh generated on the calculated component are shown in Figs 10–12. In the case of the adjusting drum, the mesh size was about 3 mm, and the numbers of TETRA6 elements and nodes in the model were equal to 377,629 and 215,431, respectively. In the case of the connector mixed with TETRA6 and HEXA20, the mesh was used. The basic size of the element was 4 mm with local refinement to 2 mm, and the total number of elements and nodes in the model was equal to 122,840 and 216,324, respectively. In the case of the movable blade with holder and tie rod, basic mixed TETRA6 and HEXA20 mesh was used. The basic size of elements was 3 mm with local refinement to 0.5 mm. The total number of elements and nodes, in this case, was equal to 128,957 and 221,964, respectively. The results of the calculation of these components are shown in Figs 13–15. The input basic material adopted for the structural elements of the fan (impeller, shaft, blade control mechanism) was steel S355 with the yield point Re = 355 MPa. Analytical calculations of the system loads showed that the mass of the moving part of the blade has a significant influence on the stress effort of the control system components. Therefore, it was assumed that the movable blade of the impeller would be made of a lightweight material, an aluminium alloy.

Based on the strength calculations, the above assumptions were verified. In the case of the adjusting drum, the local high stress was found with a maximum value of 330 MPa. This gave a safety factor of $x = 1.08$, which was considered too low. On this basis, it was found that these elements should be made of steel with a higher yield point and higher safety factors. In the case of the movable blade, the local maximum stress concentrations were obtained at the level of 298 MPa. The target material was the alloy EN AW-7075-T6 with a yield strength of Re-500 MPa, which gave the safety factor $x = 1.68$.

Fig. 10. Mesh generated on the geometrical model of the adjusting drum

DOI 10.2478/ama-2023-0002

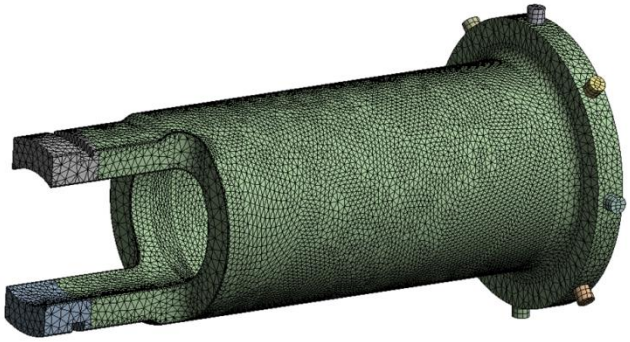

Fig. 11. Mesh generated on the geometrical model of the connector

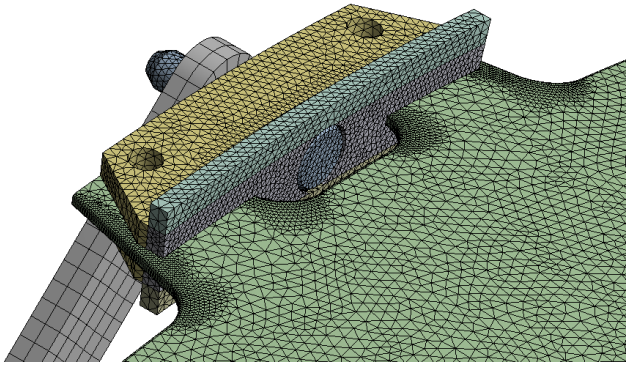

Fig. 12. Mesh generated on the geometrical model of one of the most critical assemblies in the model (movable blade connected with holder and tie rod)

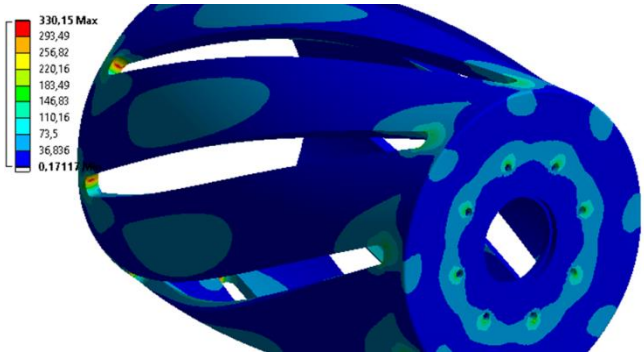

Fig. 13. Von-Mises stress distribution (in MPa) along the adjusting drum

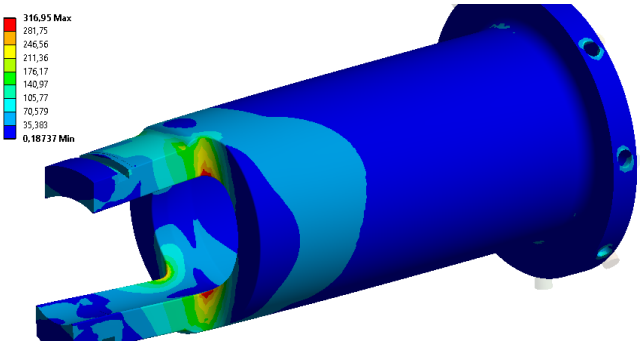

Fig. 14. Von-Mises stress distribution (in MPa) along the connector

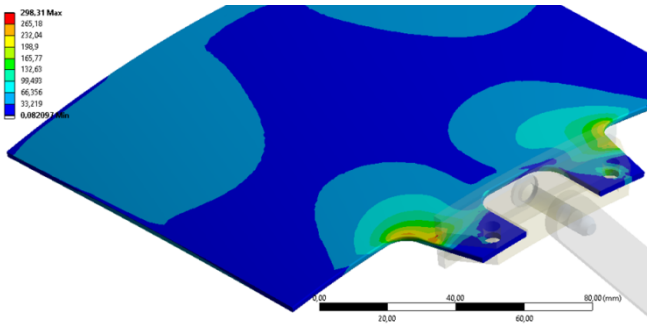

Fig. 15. Von-Mises stress distribution (in MPa) along the movable blade

3.3. CFD simulations

Numerical analysis with the use of CFD flow measurement has been realised in the early stage of the fan design process. The goal of this analysis was to preliminary evaluate fan performance curves in at least a few different positions of the movable blade. It was realised for the minimal, maximal and basic (middle) positions of the blade. In the first step, a geometrical model of the fan with the impeller in three positions was prepared. Geometrical models were simplified and in each case, the blade was without division for the fixed and movable parts. What is more, the impeller shroud and impeller hub were cut to the blade's trailing edge. The flow domain was divided into three parts: inlet zone, impeller rotating zone and outlet zone (fan volute casing zone). The calculation was carried out with the use of the 'frozen rotor approach', where terms representing the effect of the centrifugal force during impeller rotation with a rotational speed equal to $n = 1500$ rpm are taken into consideration within the impeller zone. Each domain was meshed with the use of a structural grid and the total number of elements was about five million, depending on the blade position and impeller size (grid generated in case of blade middle position is shown in Figs 16–18). To use proper turbulence model, boundary layer with first cell y+ value about 30 was created [22–24]. It means that the first cell thickness in the case of each domain was as follows:

- inlet: 0.86 mm,
- impeller: 0.63 mm,
- volute: 0.86 mm.

The growth ratio of the cells in the direction normal to the wall was in the range of 1.2–1.25.

To get the whole set of fan performance curves, each model was calculated in at least five different working points. The CFD calculations were run using a turbulence two equations model k-ω (SST), following the best practices for CFD calculation of turbomachinery equipment [25–29]. The inlet boundary condition was defined as the velocity inlet to the required volumetric flow rate. The outlet boundary condition was chosen as a pressure outlet with specified static pressure equal to 0. Additionally, turbulence intensity in the inlet and outlet sections has been chosen as 5% with the proper value of hydraulic diameter. Since maximal pressure rise was estimated at about 3500 Pa, each simulation was run as incompressible flow. The density of air in the model was defined as 1.2 kg/m³, following the standard requirements.

sciendo
DOI 10.2478/ama-2023-0002
acta mechanica et automatica, vol.17 no.1 (2023)
Special Issue "Machine Modeling and Simulations 2022"

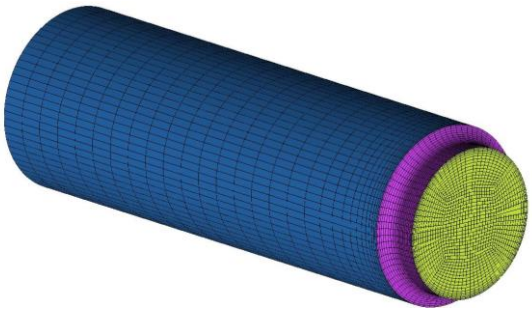

Fig. 16. CFD mesh generated on the fan inlet duct

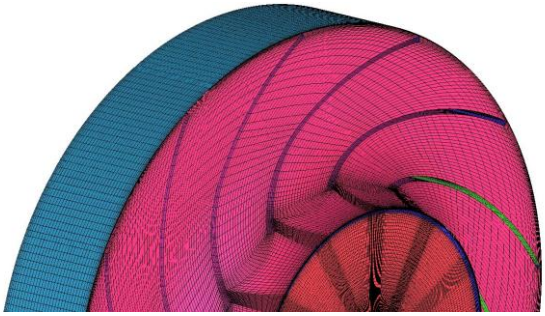

Fig. 17. CFD mesh generated on the impeller with the blade in middle position

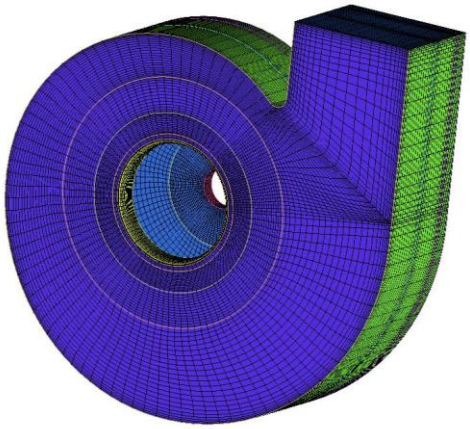

Fig. 18. CFD mesh generated on the volute casing

Any simulations were conducted until the most important flow parameters pressure and flow rate converged. As a result, a set of fan performance curves has been received (Fig. 19). These are the total pressure rise curve, shaft efficiency curve and shaft power curve in the function of volumetric flow rate. It must be underlined that each simulation was conducted with a simplified model of the fan with the movable blade. The movable and fixed blades were connected and the whole blade was only shortened or lengthened in case of minimal or maximal positions of the movable blade. This was because of the preliminary stage of the project. The main purpose of this simulation was to estimate the fan output in the expected operating range. This made it possible to define what to expect in the scope of regulation and, second, to define the energy requirements. On this basis, an appropriate electric motor was selected. At this early stage of the project, full validation of the simulations performed could not be performed due to the inability to perform tests on the prototype. However, during the simulations, the best experience during the preparation of the CFD fan model was maintained, and all the rules related to, for example, the quality and type of the mesh of the elements used were adhered to. The results of experimental tests on the prototype carried out in the final stage of the works, confirmed the results obtained from CFD simulation tests.

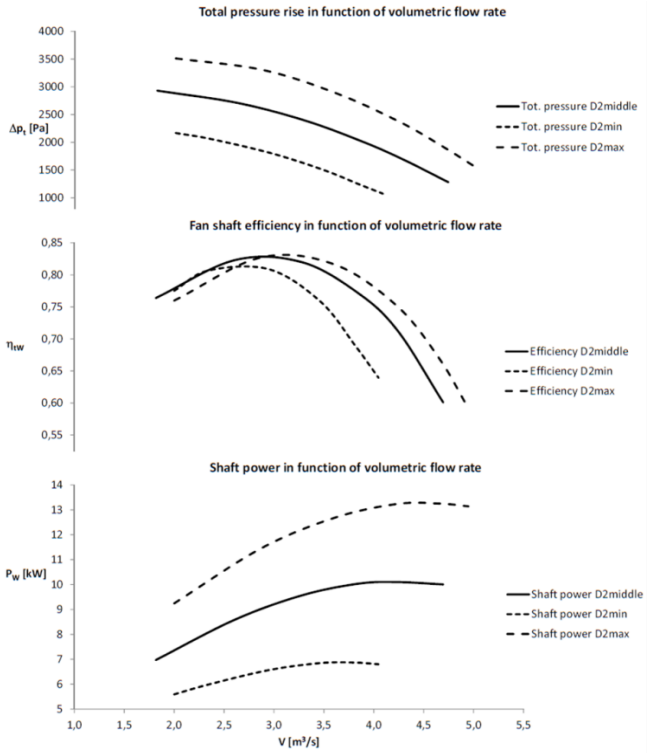

Fig. 19. Fan performance curves of the designed fan in minimal, basic (middle) and maximal movable blade positions get from CFD simulations

3.4. Modal analysis

Modal analysis is a very important step during the designing of the new rotating machinery components. During the fan operation, there are two main excitation frequencies to be considered in the dynamic safety analysis. The first frequency is the result of the rotation velocity and in the case of rotation with rotational speed 1500 rpm is equal to f_{rot} = 25 Hz. The second frequency is blade passing frequency and is equal to f_{BPF} = 300 Hz in the case of the designed fan since it is equipped with 12 blades. Modal analysis with the use of numerical techniques (FE analysis) should be performed before manufacturing the fan. Such an approach gives a chance to prevent high vibration levels and noise emissions during fan operation. Thanks to this, the higher durability of the most important rotating component as well as the bearing can be achieved [3, 4, 17–21].

In the case of a designed fan, which can be operated in different configurations of the movable blade and can also be adjusted with the use of a frequency inverter, the modal analysis can be used as a tool to find the most dangerous ranges of frequencies. Then these values can be used to prepare guidelines for the user to prevent the operation of the fan within these ranges. The designed fan needs to be verified with the blade at least in a few different blade positions between maximal and

DOI 10.2478/ama-2023-0002

minimal ones. What is more, modal analysis of a single component seems to be not a sufficient source of information about the behaviour of such a component when it works in connection with others. Because of that, a simulation of the main rotating components with the blade in minimal, maximal and middle (basic) positions has been conducted. Existing contacts between connected elements have been simplified and replaced by rigid or beam elements to ensure interaction between these components. The geometrical mixed surface and solid model of the components calculated during modal analysis are shown in Fig. 20. There is an impeller with a movable blade in a maximal position. Based on this model, a solid-shell discrete model has been prepared. What is more, the shaft was simplified and modelled with the use of a beam element. The discrete model is shown in Fig. 21. All simulations were carried out with a pre-stressed model (loads due to rotational movement with a speed of 1500 rpm and gravity forces). As a result, natural frequencies and mode shapes have been identified. These results are summarised in Table 1 and the exemplary mode shapes are shown in Figs 22–29. Beyond normal mode shapes of the impeller (torsion and bending modes), there are also visible shapes connected with the steering mechanism, especially with the tie rod since they are vulnerable to vibration because of their small bending stiffness. Many of the natural frequencies (about 300 Hz) are close to the blade passing frequency in case of impeller movement with a rotational speed of 1500 rpm. Mostly these shapes are bending of the tie rod, but not only.

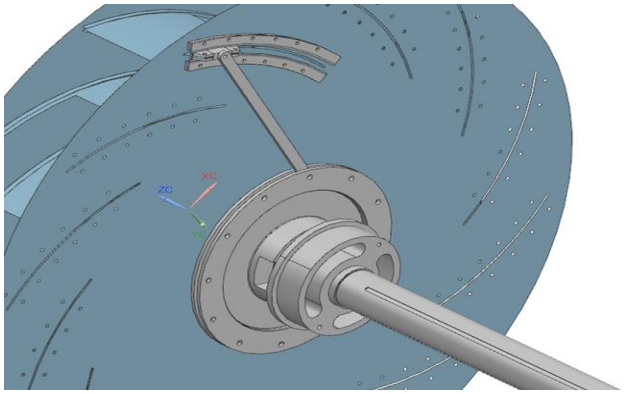

Fig. 20. Geometrical model of the impeller with adjusting mechanism and shaft with the blade in the maximal position

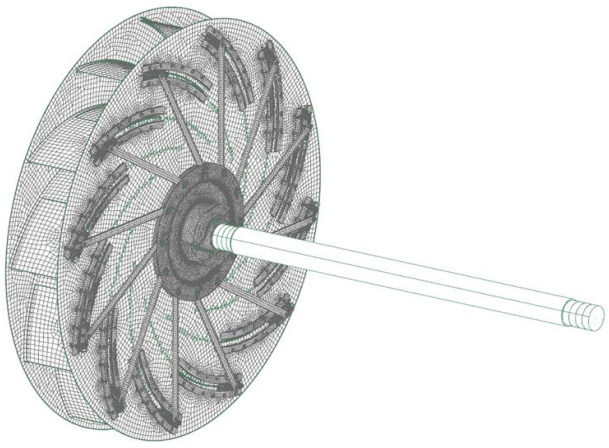

Fig. 21. Discrete model of the impeller with adjusting mechanism and shaft

Tab. 1. The results of the modal analysis of the impeller with the most important components of the regulation mechanism with the blade in minimal, maximal and basic (middle) positions

No of consecutive natural frequencies	Natural frequency with respect to the position of the movable blade (Hz)		
	Minimal	Basic (middle)	Maximal
1	29.78	29.72	29.7
2	40.88	40.42	40.7
3	40.89	40.43	40.71
4	80.45	79.82	80.41
5	218.64	246.53	258.62
6	219.16	246.71	258.74
7	243.56	256.36	261.28
8	247.46	256.79	261.45
9	247.98	282.54	288.41
10	268.59	299.45	301.85
11	268.89	300.62	302.39
12	272.22	301.01	306.46
13	273.02	301.17	308.41
14	287.98	301.33	308.44
15	293.28	305.89	309.8
16	293.54	306.05	309.98
17	306.63	307.6	312.53
18	307.57	307.62	312.55
19	307.71	308.96	313.68
20	308.13	308.98	313.79
21	308.40	309.32	314.17
22	309.97	326.3	358.85
23	309.99	326.78	359.18
24	310.75	330.89	413.46
25	310.76	333.42	413.73

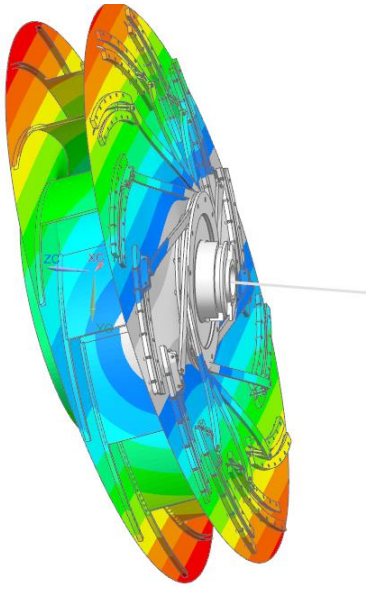

Fig. 22. Exemplary mode shape of the impeller with the blade in minimal position (2nd bending mode shape, natural frequency 40.88 Hz)

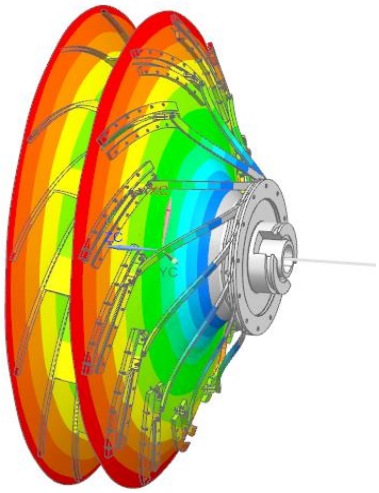

Fig. 23. Exemplary mode shape of the impeller with the blade in minimal position (4th bending mode shape, natural frequency 80.45 Hz)

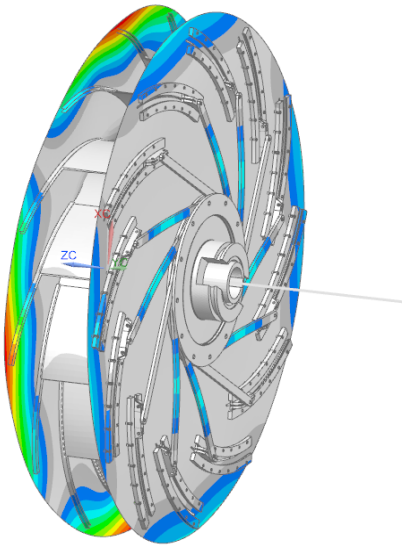

Fig. 24. Exemplary mode shape of the impeller with the blade in minimal position (15th bending mode shape, natural frequency 293.28 Hz)

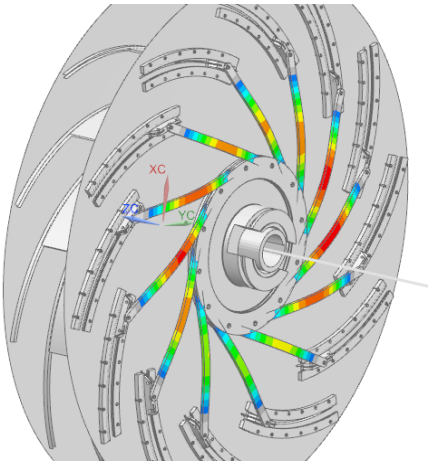

Fig. 25. Exemplary mode shape of the impeller with the blade in minimal position (17th bending mode shape, natural frequency 306.63 Hz)

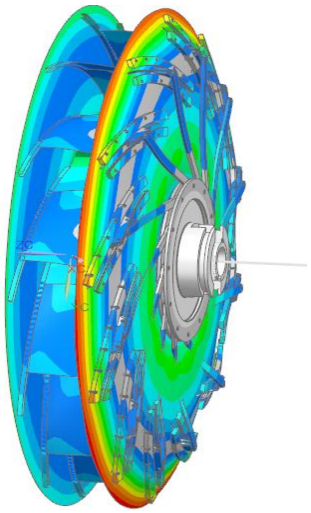

Fig. 26. Exemplary mode shape of the impeller with the blade in basic (middle) position (9th bending mode shape, natural frequency 282.54 Hz)

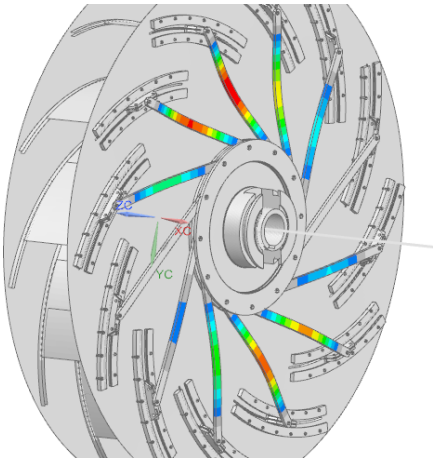

Fig. 27. Exemplary mode shape of the impeller with the blade in basic (middle) position (11th bending mode shape, natural frequency 300.62 Hz)

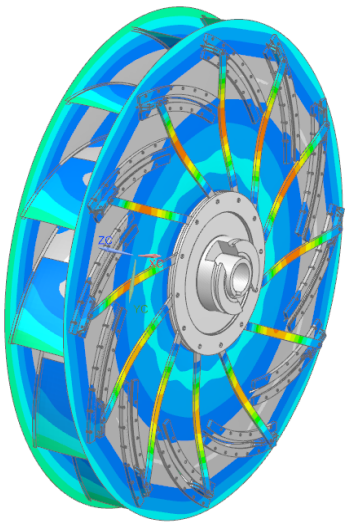

Fig. 28. Exemplary mode shape of the impeller with the blade in maximal position (9th bending mode shape, natural frequency 288.41 Hz)

DOI 10.2478/ama-2023-0002

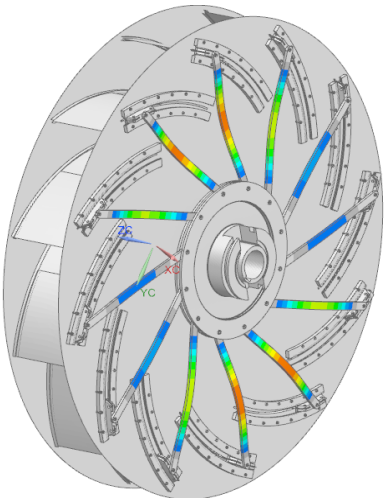

Fig. 29. Exemplary mode shape of the impeller with the blade in maximal position (10th bending mode shape, natural frequency 301.85 Hz)

4. FINAL PROJECT

The end result after the analytical and numerical calculations is the preparation of technical documentation of the prototype. Then, on this basis, its production is commissioned for further testing. Figs 30 and 31 show the developed centrifugal fan with variable impeller geometry. The change occurs by shortening and lengthening the moving part of the blade (pos. 1). This movement is carried out by using a specially designed mechanism (pos. 2), which changes the translational movement into a rotational movement.

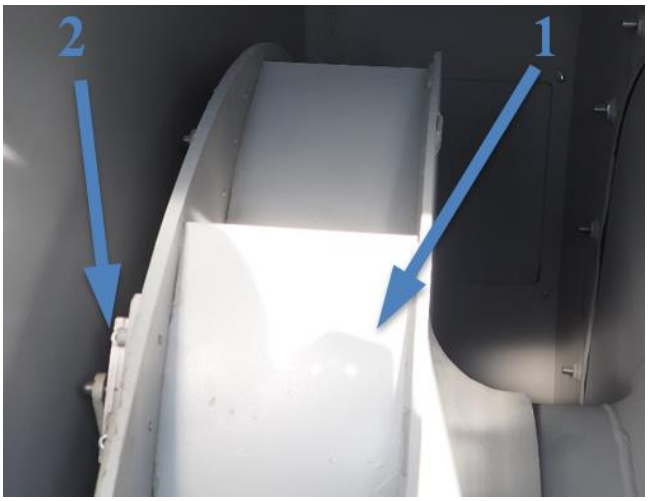

Fig. 30. Prototype of the centrifugal fan impeller with adjusting mechanism

The developed form of the finished solution allows you to change the geometry during the operation of the fan. This is possible because of the forcing mechanism (pos. 2). It has been designed to allow free rotation of the fan shaft inside the mechanism. Without this feature, it would be impossible to shorten and lengthen the blade during operation. At this stage of the project, it was necessary to verify the correctness of the work of the entire mechanism regulating the geometry of the impeller. This is a necessary step before proceeding with the field tests, which are described in the next section. The finished demonstrator is shown in Fig. 32.

Fig. 31. Steering mechanism forcing a change in rotor geometry on the prototype impeller

Fig. 32. Prototype of the centrifugal fan with variable impeller geometry

5. FIELD TEST

Test on the real object was aimed at verification of the performance and vibration level of the prototype fan. In the following subsections, the results of these measurements are summarised.

5.1. Fan performance testing

Fan performance curves measured during testing on standardised airways are used to evaluate the real capabilities of the fan. For example, based on these curves, the fan selection process is into the expected application.

A test stand to measure fan performance curves has been prepared following suitable standards [30]. It was a standard test method with an inlet-side test duct [30]. The whole stand during

measurements is shown in Fig. 33. The fact that between minimal and maximal movable blade positions, there is an infinite number of possible blade positions, measurements have been conducted only in five different positions. These are minimal, maximal and three others with an interval equal to 25% of the whole blade path. These positions have been named as pos. 0% (minimal), pos. 25% and pos. 50% (basic-middle), pos. 75% and pos. 100% (maximal). To get the data that required to draw fan performance curves according to the required standard, measurements were conducted in five different working points for each blade position. It was realised by throttling of the fan in the inlet duct. The received results showed as fan performance curves are presented in Fig. 34. These are curves of total pressure rise, shaft efficiency and shaft power in function of volumetric flow rate. The received results show that the newly designed fan has a wider range of operation with efficiency >60%. The range of the pressure regulation in the case of constant volume flow rate is about 30%, When we consider regulation along exemplary resistance curve shown in Fig. 34, fan conventional regulation range is equal to 0.145 [1, 2]. The minimal efficiency in this case is for the lowest blade position and it is about 65%. The highest efficiency is for 75% opening of the movable blade (pos. 75%) and it is about 81%.

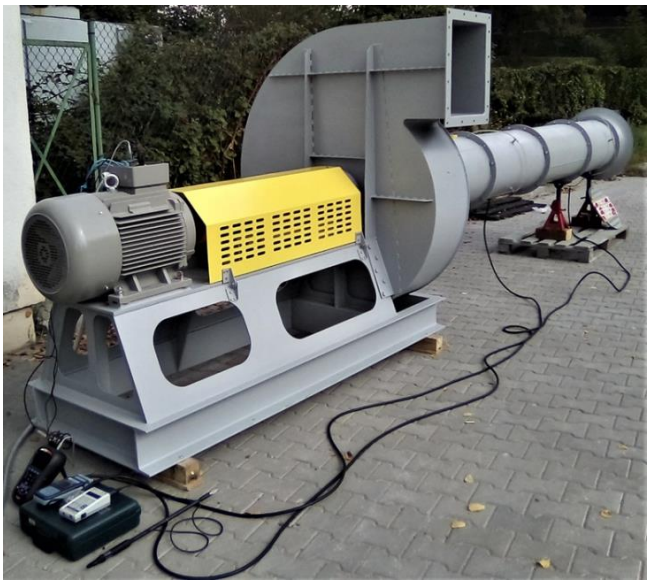

Fig. 33. Standardised airway system during measurements of the prototype fan

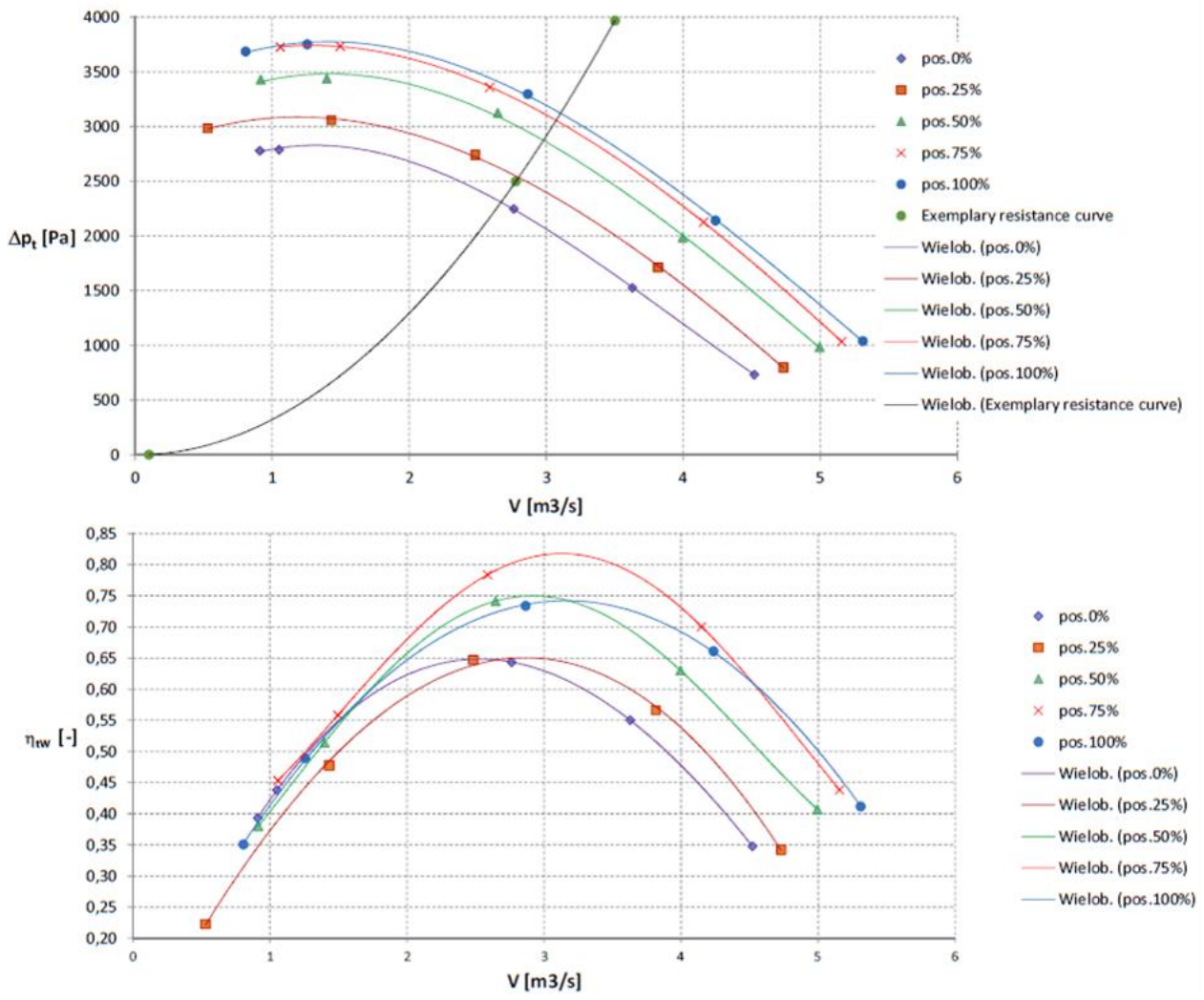

DOI 10.2478/ama-2023-0002

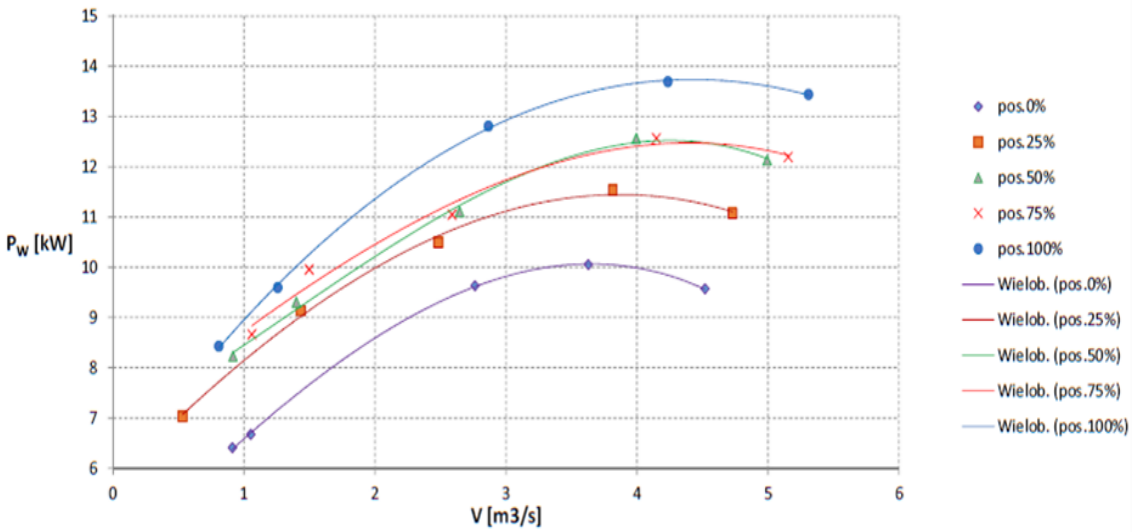

Fig. 34. Fan performance curves of the designed fan measured with the use of standardised airways. These are curves measured in 5 different positions between minimal and maximal with an interval of 25%

5.2. Vibration testing

The vibration tests were taken during regular operation with 1500 rpm.

The reference of the rotating unit rotational velocity was measured by the tachometer (laser sensor) on channel 1 (C1). The accelerometers were placed on the fixed bearing along the shaft axis (channel 2 – C2), on the fixed bearing radial horizontal direction (channel 3 – C3), on the fixed bearing radial vertical direction (channel 4 – C4), on the fan housing back wall (channel 5 – C5) and the fan housing side/cylindrical wall (channel 6 – C6). The placement of the sensor is presented in Fig. 35. The acceleration spectra are presented in Fig. 36. The vibration energy represented by the RMS factor is listed in Table 2.

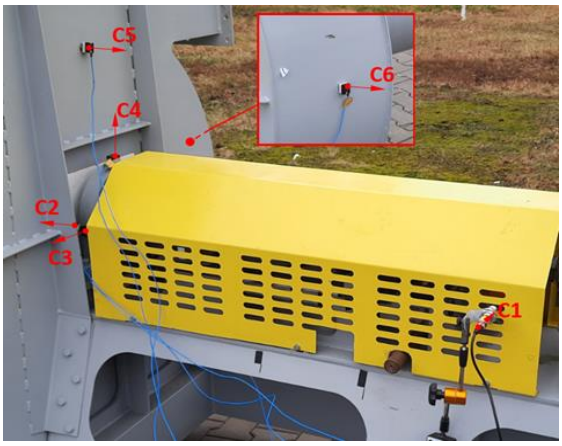

Fig. 35. Placement of the sensors during vibrations tests

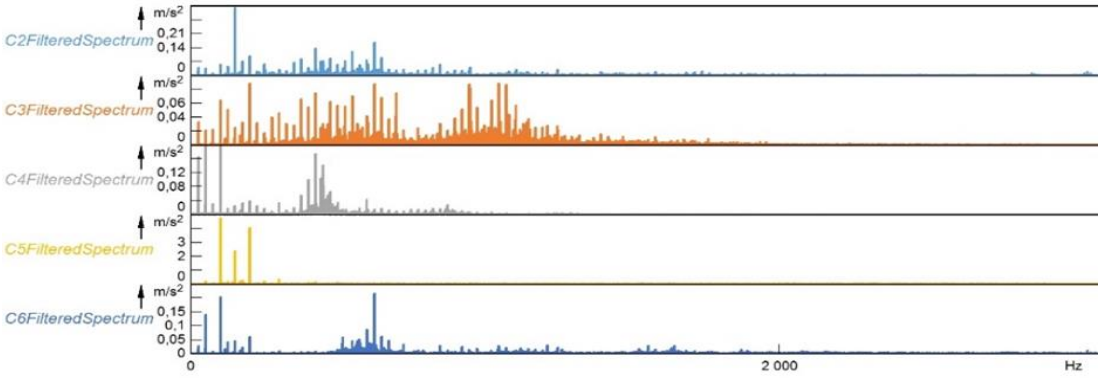

Fig. 36. Vibrations spectra

Tab. 2. Energy of the vibrations

C2	C3	C4	C5	C6
0.49	0.48	0.39	4.95	0.58

One can observe that the harmonics of the rotational velocity (25 Hz) are clearly visible at all measurement channels. As identified in the numerical modal analysis and analytical calculations, the two main ranges of possible resonances are placed at 25 Hz and 300 Hz. The analysis of the measured spectra does not provide any evidence of resonance trouble. Vibrations of the tie rods (Fig. 30) look to have the local character, as presented in the modal analysis results, and do not transfer to the bearings and casing. However, that does not exclude possible

increased wear of the tie rods and connected components in future operations.

The frequency spectrum level and the RMS value of channel 5 exceed several times the average level, but one has to keep in mind that the placement of the sensor is at the backwall casing plate of low stiffness in this particular direction.

In general, the values presented in Table 2 are satisfactory from the point of view of the requirements for industrial fans.

6. CONCLUSIONS

Summarising the above sections, the development of a fan with variable impeller geometry requires to perform two additional tasks, compared with the classic solution. The first is to design a mechanism responsible for changing the geometry. In classic solutions, this process is not needed because the geometry of the fan cannot be changed. The second step requires more calculations to verify the project. This is due to the need to verify the strength, flow and dynamic properties of different positions of the variable geometry system. In the presented solution, the test results show that thanks to this type of control of the parameters of the radial fan, it will be able to operate with about 60% greater change in total pressure increase and a 40% increase in the flow rate, and with efficiency >60% while maintaining a constant rotational speed of the rotor. Such parameters were obtained by assuming that the length of the movable part of the blade is about 30% of the length of the fixed part. Therefore, it has been shown that it is possible to significantly and effectively change the operating characteristics of the radial fan without changing the rotational speed.

The results show the great potential of such a solution. In many cases, it is possible to replace the control method by using a frequency converter, i.e., a variable rotational speed, for the proposed method of blade length control. This lowers the construction costs of fans, especially those with a higher power, where the cost of the inverter is significant. In addition, efficiency losses that occur during inverter operation are also eliminated.

REFERENCES

1. Kuczewski S. Wentylatory. Warszawa: WNT, 1978.
2. Kuczewski S. Wentylatory promieniowe. Warszawa: WNT, 1966.
3. Fortuna S. Wentylatory: podstawy teoretyczne, zagadnienia konstrukcyjno-eksploatacyjne i zastosowanie Kraków: TECHWENT, 1999.
4. Bommes L, Fricke J, Grundmann R. Ventilatoren, 2. Auflage. Essen: Vulkan-Verlag, 2002.
5. Mode F. Ventilatoranlagen: Theorie, Berechnung, Anwendung. Berlin New York: Walter de Gruyter, 1972.
6. Bohl W. Ventilatoren. Würzburg: Vogel-Buchverlag, 1983.
7. Jóźwik K, Papierski A, Sobczak K, Obidowski D, Kryłowicza W, Marciniak E, Wróbel G, Marciniak A, Wróblewski P, Kobierska A, Frącczak Ł, Podsędkowski L. Radial fan controlled with impeller movable blades – CFD investigations. Transactions of the Insitute of Fluid Flow Machinery. 2016; 131: 17-40.
8. Radwański J, Laskowski W, Lewkowicz J, Podsętkowski A. Wentylator promieniowy z końcowymi częściami łopatek wirnika nastawnymi w czasie ruchu. Polish home patent no. 52456, 1967 . (Urząd Patentowy PRL)
9. Bukowski A. Cichosza! Optymalizacja wentylatorów sposobem na ograniczenie hałasu i kosztów. Polski Przemysł, 2013.
10. Chmielarz W, Moczko P, Odyjas P, Rusiański E, Więckowski J, Wróblewski A. Wirnik wentylatora promieniowego. Polish home patent no. 234339, 2020. (Urząd Patentowy RP)
11. Miller S. Teoria maszyn i mechanizmów: analiza układow kinematycznych. Wrocław: Oficyna Wydawnicza Politechniki Wrocławskiej, 1996
12. Gronowicz A, Miller S, Twaróg W Teoria maszyn i mechanizmów: zestaw problemów analizy i projektowania. Wrocław: Oficyna Wydawnicza Politechniki Wrocławskiej, 2000
13. Zienkiewicz O C, Taylor R L, Zhu J Z. The Finite Element Method – Its Basis and Fundamentals. 6th edition. ELSEVIER, 2005.
14. Zienkiewicz O C, Taylor R L. The Finite Element Method for Solid and Structure Mechanics. 6th edition. ELSEVIER, 2005.
15. Rusiński E, Czmochowski J, Smolnicki T. Zaawansowana metoda elementów skończonych w konstrukcjach nośnych. Wrocław: Oficyna Wydawnicza Politechniki Wrocławskiej, 2000.
16. Rusiński E, Moczko P, Odyjas P, Pietrusiak D. Investigation of vibrations of a main centrifugal fanused in mine ventilation. Archives of Civil and Mechanical Engineering. 2014; 14: 569–579.
17. Cory W T W. Fans&Ventilation – A Practical Guide. Elsevier, 2005.
18. Czmochowski J, Moczko P, Odyjas P, Pietrusiak D. Test of Rotary Machines Vibrations in Steady and Unsteady States on the Basis of Large Diameter Centrifugal Fans. Eksploatacja I Niezawodność – Mainten ance and Reliability. 2014; 16(2): 211-216.
19. Uhl T. Komputerowo wspomagana identyfikacja modeli konstrukcji mechanicznych. Warszawa: WNT, 1997.
20. Randall R B. Vibration-based Condition Monitoring. A John Wiley and Sons, Ltd, 2011.
21. Rusiński E, Moczko P, Odyjas P, Więckowski J. The numerical and experimental vibrations analysis of WLS series fans designed for the use in underground mines. Proc. Int. Conf. Computer Aided Engineering (Polanica Zdrój) Lecture Notes in Mechanical Engineering (Springer). 2017; 489–504
22. ANSYS FLUENT 12.0 – Tutorial Guide (Ansys Inc.)
23. ANSYS FLUENT 12.0 – User's Guide (Ansys Inc.)
24. ANSYS Fluent Theory Guide (Ansys Inc.)
25. Cheah K W, Lee T S, Winoto S, Zhao Z M. Numerical Flow Simulation in a Centrifugal Pump at Design and Off-Design Conditions. International Journal of Rotating Machinery. 2007.
26. Engin T. Study of tip clearance effects in centrifugal fans with unshrouded impellers using computational fluid dynamics. Proceedings of the Institution of Mechanical Engineers, Part A: Journal of Power and Energy. 2006; 2220(6): 599-610.
27. Chunxi L, Ling W S, Yakui J. The performance of a centrifugal fan with enlarged impeller. Energy Conversopn and Managment, 2011; 52(8-9): 2902-2910.
28. Zawislak M. Zastosowanie numerycznej mechaniki płynów w celu poprawy sprawności przemysłowego systemu wentylacyjnego na bazie wentylatora FAWENT WP-80. Transp. Przemysłowy i Masz. Rob. 2014.
29. Ng W K, Damodaran M. Computational Flow Modeling for Optimizing Industrial Fan Performance Characteristics. Proc. Int. Conf. European Conference on Computational Fluid Dynamics ECCOMAS CFD (Egmond aan Zee, The Netherlands). 2006.
30. EN ISO 5801:2008 Industrial fans. Performance testing using standardized airways

Piotr Odyjas: https://orcid.org/0000-0002-3166-1720

Jędrzej Więckowski: https://orcid.org/0000-0002-5722-3833

Damian Pietrusiak: https://orcid.org/0000-0001-6792-9568

Przemysław Moczko: https://orcid.org/0000-0002-3819-1303